PCCP

Cite this: *Phys. Chem. Chem. Phys.*, 2012, **14**, 15562–15570

www.rsc.org/pccp

PAPER

Synthesis, characterization and sorption properties of NH_2-MIL-47†

Karen Leus,[a] Sarah Couck,[b] Matthias Vandichel,[c] Gauthier Vanhaelewyn,[d] Ying-Ya Liu,[a] Guy B. Marin,[e] Isabel Van Driessche,[f] Diederik Depla,[d] Michel Waroquier,[c] Veronique Van Speybroeck,[c] Joeri F. M. Denayer[b] and Pascal Van Der Voort*[a]

Received 26th June 2012, Accepted 1st October 2012
DOI: 10.1039/c2cp42137b

An amino functionalized vanadium-containing Metal Organic Framework, NH_2-MIL-47, has been synthesized by a hydrothermal reaction in an autoclave. Alternatively, a synthesis route *via* microwave enhanced irradiation has been optimized to accelerate the synthesis. The NH_2-MIL-47 exhibits the same topology as MIL-47, in which the V center is octahedrally coordinated. After an exchange procedure in DMF the V^{+III} center is oxidized to V^{+IV}, which is confirmed by EPR and XPS measurements. The CO_2 and CH_4 adsorption properties have been evaluated and compared to MIL-47, showing that both MOFs have an almost similar adsorption capacity and affinity for CO_2. DFT-based molecular modeling calculations were performed to obtain more insight into the adsorption positions for CO_2 in NH_2-MIL-47. Furthermore our calculated adsorption enthalpies agree well with the experimental values.

1. Introduction

Metal Organic Frameworks (MOFs) are crystalline porous solids built up by metal atoms linked together by multifunctional organic ligands. The possibility of designing a MOF with a desired structure, pore size and shape has made them very attractive in many applications. MOFs have been extensively studied for gas storage and separations,[1–18] catalysis[19–27] and luminescence.[28] Also in biomedical applications they become more and more a subject of interest.[29] The rigidity of the structure allows further functionalization without changing the original topology. Thus, a series of functional groups can be grafted onto the linker, giving perspectives for different applications. The prototype, MOF-5, constructed from octahedral Zn–O–C clusters and benzene linkers, was used to demonstrate that its three-dimensional porous system can be functionalized with the organic groups –Br, $–NH_2$, $–OC_3H_7$, $–OC_5H_{11}$, $–C_2H_4$, and $–C_4H_4$.[30] Recently, Biswas *et al.* reported an isoreticular series of Al–MIL-53-X (X = Cl, Br, CH_3, NO_2, OH).[31] Another paper reports on the isoreticular series of UiO-66 with an extra NH_2, NO_2 or Br substituent on the organic linker compared to the parent MOF.[32] These extra functional groups, embedded in the structure, can have a significant effect on the outcome for many applications ranging from adsorption to catalysis. The functionalization of porous materials with $–NH_2$ groups is of particular interest for the adsorptive separation of CO_2. For silica-based materials it was already demonstrated that functionalization of the surface of the mesopores with $–NH_2$ groups enhances the affinity toward CO_2 adsorption. This points to a strong interaction between CO_2 and the amino groups in the pores. Sometimes this even resulted in chemisorption, with the formation of carbonate, bicarbonate or carbamate species.[33–38]

For MOF materials, the effect of $–NH_2$ groups is less straightforward and is still the subject of many discussions.[39,40] For IRMOF-3 it was shown that the amino functionalization only had a marginal effect on the CO_2 sorption capacity and selectivity.[39,40] Arstad *et al.* prepared three amino functionalized materials (USO-1-Al, USO-2-Ni, and USO-3-In) and they concluded that the capacity toward CO_2 is increased in comparison with the non-functionalized materials.[41] Pure phase amine functionalized MIL-101(Al) has been synthesized

[a] *Department of Inorganic and Physical Chemistry, Center for Ordered Materials, Organometallics and Catalysis, Ghent University, Krijgslaan 281-S3, 9000 Ghent, Belgium. E-mail: pascal.vandervoort@ugent.be; Tel: +32 964 44 42*
[b] *Vrije Universiteit Brussel, Department of Chemical Engineering, Belgium*
[c] *Center for Molecular Modeling, Ghent University, Technologiepark 903, 9052 Zwijnaarde, Belgium*
[d] *Department of Solid State Sciences, Ghent University, Krijgslaan 281-S1, 9000 Ghent, Belgium*
[e] *Laboratory for Chemical Technology, Ghent University, Krijgslaan 281-S5, 9000 Ghent, Belgium*
[f] *Department of Inorganic and Physical Chemistry, Ghent University, Sol-gel Center for Research on Inorganic Powders and Thin films Synthesis (SCRiPTS), Krijgslaan 281-S3, 9000 Gent, Belgium*

† Electronic supplementary information (ESI) available: Nitrogen adsorption isotherms of NH_2-MIL-47 and MIL-47. Detailed information about the breakthrough setup, pulse gas chromatography measurements and VASP calculations. Adsorption geometries of CO_2 and CH_4 on the (amino-) terephthalate linker, NH_2-MIL-47 and MIL-47. See DOI: 10.1039/c2cp42137b

in the work of Serra-Crespo *et al.*[42] The separation properties have been assessed in terms of single component adsorption and mixture separation. The authors found that NH_2-MIL-101(Al) is an excellent candidate for the selective adsorption of CO_2 from methane and N_2. The functionalized material also displays a high CO_2 capacity, but lower than the unfunctionalized MIL-101 with Cr instead of Al. On the other hand NH_2-MIL-101(Al) performs better in CO_2/CH_4 separation than MIL-101(Cr) at low CO_2 pressures.[42] An amine-functionalized ZIF (ZIF-96) displays again higher CO_2 adsorption capacities.[43]

In the specific case of MIL-53(Al), the functionalization of the framework with $-NH_2$ groups leads to a drastic increase in selectivity for CO_2 in mixtures with CH_4 as compared to the non-functionalized material, but this is not caused by a direct interaction (chemisorption) between CO_2 and the NH_2 groups.[44–46] Lescouet *et al.* have shown that the adsorption capacity varies according to the fraction of the amine functionalized linker.[47]

Furthermore, the flexibility of the frameworks plays also an important role in adsorption processes. Several papers studied the difference in adsorption behavior between the rigid MIL-47 in comparison to the flexible and breathing MIL-53. In a recent paper of Trung *et al.*,[48] MIL-53(Cr) and MIL-47(V) were studied for the adsorption of the apolar species, *n*-hexane and *n*-nonane. While MIL-53(Cr) exhibits a sub-step during the sorption process explained by a structural transition of the framework, one obtains a I-type isotherm for MIL-47 as typically observed for non-flexible microporous materials.[48,49] In the recent paper of Leclerc *et al.*,[49] it has been shown that the oxidation state of vanadium is decisive for the MIL-47 to show a breathing effect. If the vanadium resides in a $+III$ state, a similar breathing effect as in MIL-53 has been observed whereas the presence of V^{+IV} centers inhibits the flexibility to a large extent.[49] Conversely, the use of amine groups may also inhibit CO_2 adsorption, as observed on the modified MIL-53(Fe), when strong bonds maintain the structure in its closed form.[50]

To the best of our knowledge, amino functionalized MIL-47 has not yet been investigated. As can be seen from Fig. 1, NH_2-MIL-47 has a three-dimensional framework, where each V^{+IV} center is coordinated to four oxygen atoms from four carboxylate groups, and to two oxygen atoms on the O–V–O axis, thus forming a saturated octahedral coordination node.

The parent MIL-47 has already demonstrated to possess good catalytic and adsorption properties.[24,25,49,51–53]

In this contribution, we report on the synthesis and characterization of the amino functionalized V-MOF with a MIL-47 topology. The CO_2 and CH_4 adsorption properties of this NH_2-MIL-47 have been investigated and are compared to the parent MIL-47. Theoretical modeling can assist us in explaining the differences observed in the adsorption behavior between both materials.

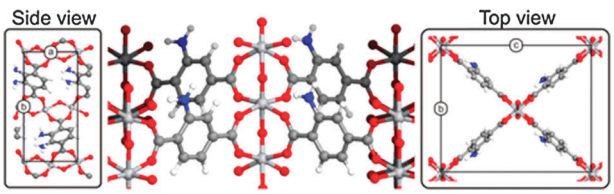

Fig. 1 Side, front and top view of the structure of NH_2-MIL-47.

2. Experimental section

2.1 Synthesis of NH_2-MIL-47 and MIL-47

NH_2-MIL-47 *as* has been synthesized by 2 possible routes. The first route was carried out in an autoclave. The molar ratio of VCl_3/2-aminoterephthalic acid/H_2O was 1/1/100. Typically 9 mmol vanadium(III)chloride and 9 mmol 2-aminoterephthalic acid were mixed in a Teflon insert with 16.60 mL H_2O and placed in an autoclave for 4 days at 150 °C. Moreover, to accelerate the synthesis time, a procedure under microwave irradiation has been developed. For the microwave assisted synthesis 1.7 mmol VCl_3 was mixed with 1.7 mmol 2-aminoterephthalic acid in 3.02 mL H_2O. The reaction was carried out at 150 °C for 20 minutes, reducing the synthesis time significantly from 4 days to 20 minutes without loss in crystallinity. In a second step, an exchange procedure in DMF at 125 °C has been carried out for 90 minutes to remove the unreacted linker. MIL-47 was synthesized according to a synthesis route described in the literature.[54]

2.2 Characterization

All the chemicals were bought from Sigma Aldrich and used without further purification. The microwave assisted synthesis was carried out in a microwave synthesizer (Discover, CEM Inc.). Scanning electron microscopy (SEM) images were taken on a FEI Quanta 200FEG microscope with 4 nm resolution operating at 30 kV. Nitrogen adsorption experiments were measured at −196 °C using a Belsorp mini II gas analyzer. Diffuse Reflectance Infrared Fourier Transform Spectroscopy (DRIFTS) was measured on a Thermo Nicolet 6700 FT-IR spectrometer equipped with a N_2 cooled MCT-A (mercury–cadmium–tellurium) detector. Thermo Gravimetric Analysis (TGA) was performed on an SDT 2960 from TA Instruments. X-ray powder diffraction (XRPD) patterns were collected on an ARL X'TRA X-ray diffractometer with Cu Kα radiation of 0.15418 nm wavelength and a solid state detector. Elemental analyses (C, H, N) were performed on a Thermo Scientific Flash 2000 CHNS-O Analyzer. The EPR spectra were recorded at room temperature using a Bruker ESP300E X-band spectrometer with a maximum microwave power of 200 mW. The measurements were performed using a Bruker ER 4114-HT (high temperature) cavity. The latter is a cylindrical cavity resonating in the TE_{011} mode. The magnetic field was modulated at 100 kHz with a peak-to-peak amplitude of 0.1 mT. The spectra were averaged 4 times with a sweep time of 335.5 s and a time constant of 81.92 ms. The magnetic field sweep width was 1.5 T and the center field was set close to the free electron *g*-value (2.0023). All spectra contained 2048 data points. The samples were transferred into ER 222 G-type quartz tubes with an outer diameter of 4 mm for recording. The samples masses were about 20 mg. All EPR spectra have been normalized to a microwave frequency of 9.51 GHz for comparison. The magnetic field and microwave frequency were measured using a Bruker ER035M gaussmeter and a HP 5350 B microwave frequency counter, respectively. The XPS measurements were recorded on a X-ray photoelectron spectroscopy S-Probe XPS spectrometer with monochromated Al (1486 eV) exciting radiation from Surface Science Instruments (VG). The powder was pressed into a Sn substrate.

A flood gun set at 3 eV and a Ni grid placed 3 mm above the sample surface were used for charge compensation. A survey spectrum and details of the V 2p, O 1s and C 1s region were recorded. In short, subsequent measurements of the V2p region show no signs of peak shift during the measurement. The binding energy was calculated with respect to the C 1s adventitious carbon fixed at 284.6 eV.

2.3 Adsorption tests

Adsorption isotherms of pure CO_2 (purity of 99.99%) and CH_4 (purity of 99.95%) were determined at 30 °C, using the volumetric technique. About 0.5 g of MIL-47 or NH_2-MIL-47 was loaded into the sample container. Prior to the measurement the sample was out-gassed by heating it up to 80 °C under vacuum.

Breakthrough experiments have been performed using a column with a length of 30 cm and an internal diameter of 0.216 cm packed with 600 mg of MOF pellets. Pellets were obtained by pressing the powder to a solid disk, crushing the disk followed by sieving to the desired fraction of 500–630 μm. The adsorption capacity was calculated *via* the method of Malek and Farooq (1996).[55] The same column was used for obtaining pulse gas chromatographic (pulse GC) data, *i.e.* Henry constants and adsorption enthalpies of CO_2 and CH_4. More details of this technique are reported elsewhere.[56] Additional information about the breakthrough setup and the pulse gas chromatography measurements are given in the ESI.†

2.4 Computational details

The computational study comprises two types of *ab initio* calculations: first non-periodic cluster calculations to obtain initial insight into the active site of adsorption on the terephthalic linkers with and without amino functionalization. Second, periodic calculations on the parent MIL-47 and NH_2-MIL-47 were done. The cluster geometries were optimized with the Gaussian 09 package[57] using Density Functional Theory (DFT) with the hybrid M06-2X functional[58,59] to study the initial adsorption of CH_4 and CO_2 on both linkers. This functional is the best choice to quantify the interactions of CH_4 and CO_2 with the organic linkers because it is utilized especially for medium range non-covalent interactions. The double-zeta Pople basis set 6-311+g(d,p) was applied. The optimized clusters were confirmed to be true minima on the potential energy surface by performing a vibrational frequency analysis, which confirmed that only positive frequencies were present. Afterwards, van der Waals corrections for the M06-2X functional were added to the energy.[60,61] The thermal corrections were added to the energy to determine the enthalpy, by an in-house developed software module TAMkin.[62]

Secondly, the adsorbate molecules CH_4 and CO_2 were placed within the periodic V-MOF structures, in a position that corresponds to the most optimal geometries obtained with the cluster calculations. The geometry of the periodic system with inclusion of the guest molecules has been optimized by means of the Vienna *Ab Initio* Simulation Package (VASP)[63–66] making use of the PBE exchange correlation functional.[67,68] For more details we refer to the Computational Section of the ESI.† In order to prevent self interactions between the adsorbates in neighbouring cells the unit cell has been doubled along the *a* direction. The orientation of the amino group on the linkers is taken as in the crystallographic structure of NH_2-MIL-53(Fe) as reported elsewhere.[69]

3. Results and discussion

3.1 Structure analysis

XRPD measurements (Bragg–Brentano configuration) of both V-MOFs were executed. Based on the obtained XRPD spectra the corresponding *d*-spacings were calculated. The comparison between both samples together with the lines calculated from the MIL-47 structure as published by Barthelet *et al.*[54] (shown in grey) is presented in Fig. 2.

Detailed analysis of both spectra shows that 20 lines of 21 lines of the modified MIL-47 structure correspond (within the error of the measurement) with the MIL-47 lines for which 26 lines were detected. This nice agreement is shown in Fig. 2 (top). From this XRPD analysis one can conclude that the molecular structure of the modified MIL-47 is very similar to the original MIL-47 structure. The addition of the amino group hardly influences the molecular structure. The *as*-synthesized sample is formulated as $V^{+III}OH(C_8H_5NO_4)\cdot x(C_8H_7NO_4)$ ($x \sim 0.58$) on the basis of the elemental analysis (calcd: C 43.11, H 2.88, N 6.28%; found: C 43.10, H 2.86, N 6.39%). After exchange with DMF, the elemental formula is $V^{+IV}O(C_8H_5NO_4)$ denoted as NH_2-MIL-47.

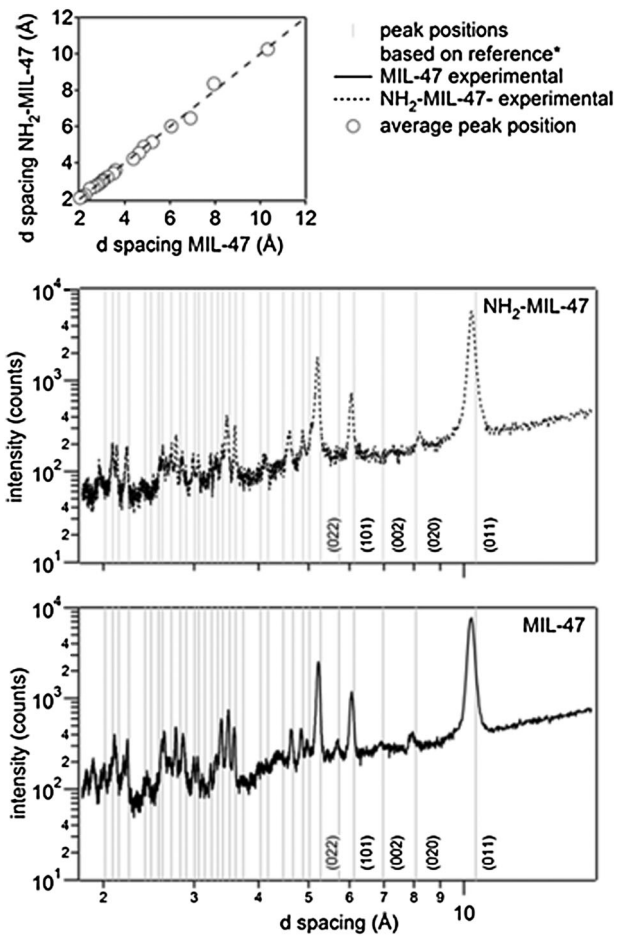

Fig. 2 Calculated *d*-spacings for MIL-47 and NH_2-MIL-47 (ref. 54).

3.2 N_2 sorption measurements

Major efforts have been done to find the appropriate pretreatment of the V-MOF. An exchange procedure in DMF has been optimized to remove unreacted linkers and to obtain the highest surface area without loss of the integrity of the framework. The results of the exchange procedure are summarized in Table 1.

The optimal surface area was obtained at an exchange temperature of 125 °C for 90 minutes. Exchange experiments at 150 °C caused already significant damage to the structural integrity. If the exchange experiment was carried out at 150 °C for 240 minutes the MOF structure was completely dissolved. However, at a lower temperature (100 °C), we were unable to completely remove the free linker from the pores. Longer exchange times at this temperature gave no improvement. An exchange temperature of 125 °C for 90 minutes gave the highest surface area without structural damage, whereas a longer exchange time at 125 °C leads already to damage of the structure. Furthermore, the presence of water and long exposure times to ambient conditions (in the absence of any solvent) should be avoided as gradual decomposition will take place. The Langmuir surface area of MIL-47 was approximately 1200 $m^2\ g^{-1}$, which was comparable to the value reported in the literature.[54] The BET values, determined in the P/P_0 pressure interval between 0.05 and 0.2, for MIL-47 and NH_2-MIL-47 are, respectively, 809 $m^2\ g^{-1}$ and 535 $m^2\ g^{-1}$. The isotherms of MIL-47 and the optimized NH_2-MIL-47 are shown in Fig. S2 in the ESI.†

3.3 Thermal behavior

To examine the thermal stability of NH_2-MIL-47, a TGA experiment has been carried out with a heating rate of 2 °C min^{-1} in air. The resulting TGA curve is shown in Fig. 3. Prior to this measurement the sample was dried under vacuum to remove DMF and H_2O molecules.

As can be seen from this figure, the first and only weight loss starts at 280 °C, indicating that the V-MOF is stable up to 280 °C. Afterwards, the framework starts to decompose. The thermostability is in agreement with the earlier reported MIL-47.[54] Thus, the introduction of functional groups does not influence the thermal stability. Moreover, we can conclude that the pretreatment step was successful to remove occluded guest molecules.

3.4 Determination of the oxidation state

EPR measurements were performed to determine the oxidation state of the V in NH_2-MIL-47 *as* and NH_2-MIL-47.

Table 1 Optimization of the exchange procedure in DMF for NH_2-MIL-47

Time/minutes	Exchange temperature/°C	Langmuir surface area/$m^2\ g^{-1}$
90	150	572
240	150	—
60	100	287
90	100	280
60	125	257
90	125	672
150	125	647
180	125	386

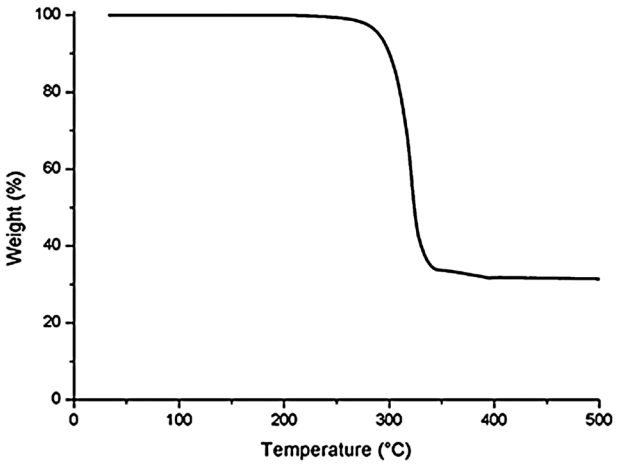

Fig. 3 TGA curve of NH_2-MIL-47 obtained under an air flow with a heating rate of 2 °C min^{-1}.

The measurements were carried out with a rectangular High Temperature EPR Cavity (HTC). In Fig. 4, the spectra of both samples are shown.

As expected, the NH_2-MIL-47 *as* spectrum does not show any signal due to V^{+IV}. From this observation one can conclude that the metal is in the +III oxidation state. On the other hand, a manifest signal is observed in the NH_2-MIL-47 spectrum which can be attributed to V^{+IV}. The latter is the result of the exchange procedure in DMF. In the recent report of Leclerc *et al.* it was already suggested that the presence of DMF molecules could oxidize the V center in MIL-47.[49] Moreover, both observations are in agreement with the proposed structural formula obtained from elemental analysis. In addition, XPS measurements were performed (Fig. 5). The binding energy for a V2p3/2 peak in NH_2-MIL-47 is observed at 516.8 eV. This coincides with the spectrum for MIL-47 (BE: 516.8 eV) and $VO(acac)_2$ (BE: 516.2 eV) both known as V^{+IV}.[54,70]

3.5 IR and SEM measurements

In Fig. 6, the DRIFT spectrum of NH_2-MIL-47 *as* and NH_2-MIL-47 is shown. A distinct difference between both spectra is the broad band at around 3630–3680 cm^{-1}, which is only

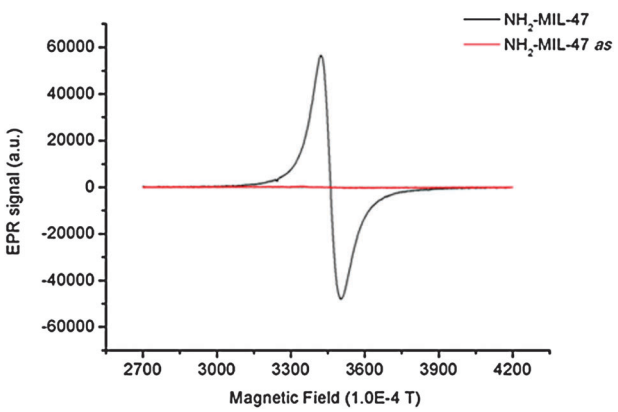

Fig. 4 EPR X-band spectrum of NH_2-MIL-47 *as* (red) and NH_2-MIL-47 (black).

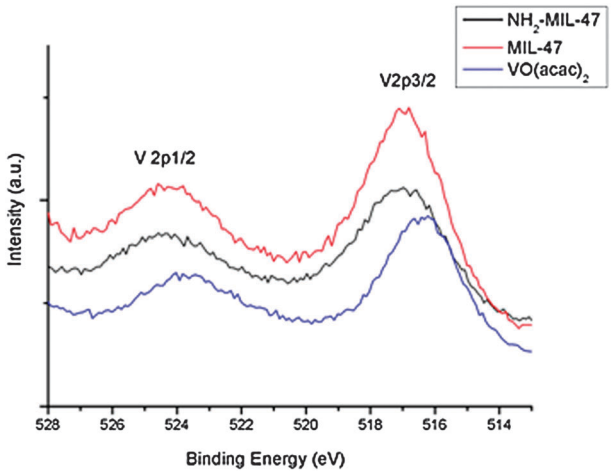

Fig. 5 XPS spectra of V2p3/2 and V2p1/2 region of MIL-47, NH_2-MIL-47 and $VO(acac)_2$.

present in the *as*-synthesized sample. This rather broad band represents a combination of both the stretching vibration of the μ_2-OH group (the $V^{III}O$–H) and the free OH groups of the trapped linker.[69] The total disappearance of this band in the NH_2-MIL-47 clearly demonstrates the complete removal of the free linker after the optimized exchange procedure and the oxidation of the $V^{III}O$–H towards V^{IV}=O groups.

The doublet at 3494 and 3386 cm^{-1} corresponds to the asymmetrical and symmetrical stretching of the amine groups, the vibration at 1630 cm^{-1} can be attributed to the N–H bending (scissoring) vibration. The C–N stretching absorption of the aromatic amines is located at 1338 cm^{-1}.[21,32] Typical vibrations, due to the benzene linker can be observed: 1510–1450 cm^{-1} (aromatic ring stretch), 1225–950 cm^{-1} (aromatic C–H in plane bend) and 900–670 cm^{-1} (aromatic C–H out of plane bend).[71] The vibrations in the region 1597–1616 cm^{-1} and 1415–1463 cm^{-1} can be assigned to the asymmetric and symmetric –CO_2 stretching vibrations respectively.[72]

In Fig. 7, the SEM pictures of the materials obtained *via* microwave and autoclave procedure are presented. It can be seen that the structure, crystal size and morphology of the materials obtained *via* both synthesis routes are very similar (Fig. 7a and c).

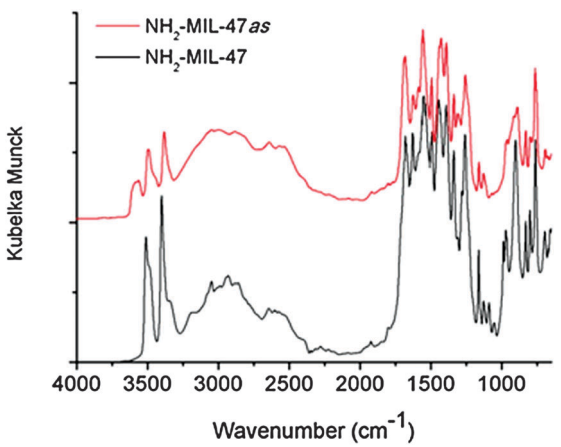

Fig. 6 DRIFT spectrum of NH_2-MIL-47 *as* (top) and NH_2-MIL-47 (bottom).

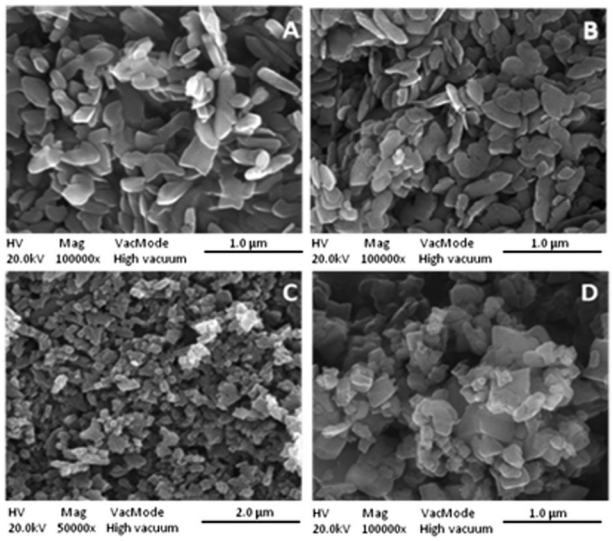

Fig. 7 SEM pictures of NH_2-MIL-47: (A) synthesized *via* autoclave, (B) after exchange *via* autoclave synthesis, (C) synthesized *via* microwave and (D) after exchange *via* microwave synthesis.

There are no significant changes observed for the materials after the exchange procedure compared to the non-treated sample (Fig. 7b and d). It is hard to give an exact size of the crystals because of the very broad crystal size distribution.

3.6 Adsorption tests: experimental and computational results

Adsorption isotherms of CO_2 and CH_4 on MIL-47 and NH_2-MIL-47 are displayed in Fig. 8. The experimentally obtained isotherms for CO_2 and CH_4 on MIL-47 show a somewhat lower capacity than was previously reported. The literature specifies a capacity for CO_2 and CH_4 of 10.1 and 5.5 mmol g^{-1}, respectively, compared to 7.7 and 4.1 mmol g^{-1} obtained in this study.[53,73] This difference should be attributed to differences in preparation methods and sample pretreatment, resulting in different micropore volumes. The calculated micropore volume for this material is 0.40 ml g^{-1} while for MIL-47 in the literature it is 0.46 ml g^{-1}.[54]

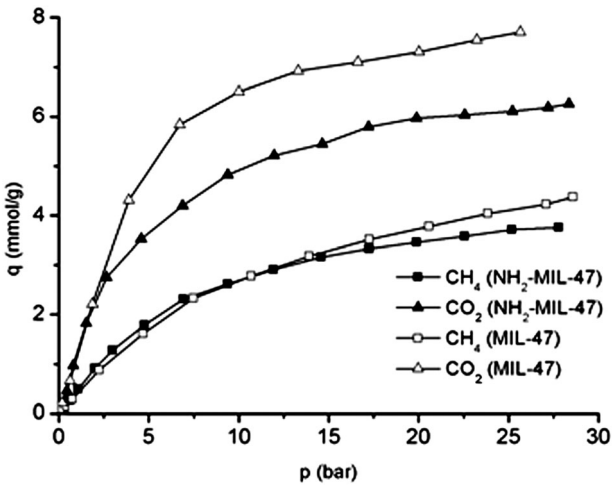

Fig. 8 Adsorption isotherms of CO_2 and CH_4 on MIL-47 (open symbols) and NH_2-MIL-47 (closed symbols) at 30 °C.

Table 2 Adsorption enthalpy (ΔH), Henry constant (K') at 30 °C of CO_2 and CH_4 and zero coverage separation factor ($\alpha_{K'}$) defined as the ratio of Henry adsorption constants of CO_2 over CH_4

	ΔH/kJ mol^{-1}		K'/mol kg^{-1} Pa^{-1}		
	CO_2	CH_4	CO_2	CH_4	$\alpha_{K'}$
MIL-47	−17.8	−11.1	1.19×10^{-5}	4.68×10^{-6}	2.5
NH_2-MIL-47	−22.0	−13.0	9.83×10^{-6}	2.65×10^{-6}	3.7

An interesting observation is the decrease in capacity (per gram adsorbent) for the amino version of the material, corresponding to 20% for CO_2 and 10% for CH_4 at 25 bar. This is in agreement with other amino functionalized MOFs[42,44,46] where a capacity drop has also taken place per mass of sample. The presence of free-standing amino-groups in the pores results in a decrease in the available pore volume. Even more interesting is that the isotherms on both materials strongly coincide in the low-pressure regime; thus the presence of $-NH_2$ groups does not result in a significant increase in affinity for CO_2 or CH_4. This is confirmed by low coverage pulse-chromatography experiments. As shown in Table 2, adsorption enthalpies, Henry adsorption constants and separation factors of CO_2 and CH_4 are comparable on both materials. This strongly differs from what is observed with the MIL-53(Al) material, where functionalization with $-NH_2$ groups results in an increase in CO_2 adsorption enthalpy of 18 kJ mol^{-1} and a multiplication of the CO_2/CH_4 separation factor by orders of magnitude.[44,46] This is related to the structure of the materials. The pore size in the low coverage area can be estimated by using the pulse gas chromatographic technique.[74] In the paper of Couck *et al.* it was shown that the MIL-53 structure is probably in the large pore (lp) form when performing low coverage experiments[75] while NH_2-MIL-53 has narrower pores in this low coverage region.[46,75] The narrower pore size is the reason for the higher adsorption enthalpy present in NH_2-MIL-53. As for MIL-47, it is known that this material does not show a flexible behavior under the present experimental conditions, meaning that MIL-47 and MIL-53 have the same adsorption properties in the low coverage domain. Also NH_2-MIL-47 does not show flexibility and as a consequence behaves the same as its parent material MIL-47.

Finally, the adsorption behavior of the parent MIL-47 and functionalized form of MIL-47 was evaluated in breakthrough adsorption experiments, in which CO_2/CH_4 mixtures of different composition, at a total pressure of 1 bar, were separated. Fig. 9 shows the amount of adsorbed CO_2 and CH_4 and the separation factor as a function of mixture composition. Capacity (per mass) for both CO_2 and CH_4, is slightly lower on NH_2-MIL-47 than on MIL-47. Again the selectivity, calculated from the breakthrough experiments, is comparable on both materials and is also in good agreement with the Henry selectivity (Table 2).

In addition to the experiments, the adsorption strength of CH_4 and CO_2 within the materials MIL-47 and NH_2-MIL-47 is investigated theoretically. Ramsahye *et al.* studied the adsorption behaviour of CO_2 in the unsubstituted materials MIL-53(Al,Cr) and MIL-47(V). By means of periodic DFT calculations on the MIL-47(V) they concluded that there are no preferential adsorption sites for CO_2.[76] In a second

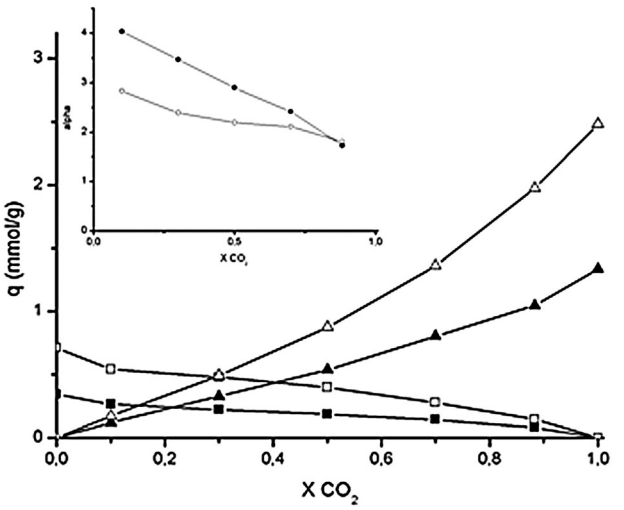

Fig. 9 Adsorption capacity for NH_2-MIL-47 (closed symbols: q CH_4 (■) and q CO_2 (▲)) and MIL-47 (open symbols: q CH_4 (□) and q CO_2 (Δ)). In the inset the selectivity for MIL-47 (○) and NH_2-MIL-47 (●) obtained *via* breakthrough experiments at 30 °C and at a total pressure of 1 bar is shown.

publication, previous authors used grand canonical Monte Carlo simulations to study the adsorption mechanism. These simulations were based on partial atomic charges extracted from periodic DFT calculations and interatomic potentials between the adsorbate and host framework.[77] Simulation of adsorption phenomena can indeed be performed using molecular dynamics and Monte Carlo simulations with suitable force fields providing us information on the distribution on the position of adsorbates within the framework and giving average adsorption data. The derivation of a proper force field is a non-trivial task and is beyond the scope of this study. This is especially true for the derivation of polarisable force fields for which no standard is available.[78,79] Herein, we performed static calculations, based on DFT and complemented with dispersion corrections, to study the qualitative differences between adsorbate–host interactions. The computational protocol is outlined in Section 2.4. A large number of adsorption structures have been investigated in the finite cluster model in order to determine the most stable configuration of the absorbate with respect to the linker. The most favorable positions are displayed in Fig. 10, both for CH_4 and CO_2. The amino group has the largest effect on the position of the CO_2 adsorbate. The polar character of CO_2 lies at the origin of a stronger electrostatic attractive interaction between the adsorbate carbon and the negative charge of the nitrogen.

The electronic adsorption energy ΔE and adsorption enthalpy ΔH_{30} at 30 °C for both the terephthalic linkers and full periodic MIL-47 type materials are tabulated in Table 3. For both adsorbates the adsorption is stronger on the amino functionalized linker and CO_2 is more adsorbed than CH_4 by about 7 kJ mol^{-1}. Qualitatively, this is in nice agreement with the experiment (Table 2). When taking into account the full topology of the MIL-47 the qualitative differences between CO_2 and CH_4 remain nearly the same, although overall the guest molecules are strongly adsorbed. This is probably the result of additional dispersion interactions between the adsorbate

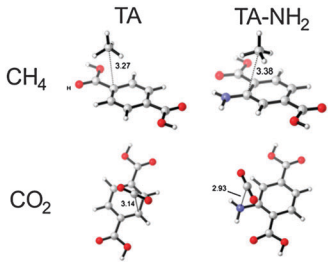

Fig. 10 An overview of the most stable adsorption positions of CO_2 and CH_4 on terephthalic acid (TA) and 2-aminoterephthalic acid (TA–NH_2) (cluster model). Shortest distances between the carbon of the adsorbate and the nearest linker atom are displayed in Ångström.

Table 3 The calculated electronic adsorption energy (ΔE in kJ mol^{-1}) and adsorption enthalpy at 30 °C (ΔH_{30} in kJ mol^{-1}). Unit cell parameters in the periodic calculations have been optimized for the parent MIL-47 and for the NH_2-MIL-47 (NH_2–TA represents the 2-aminoterephthalic acid linker and TA the terephthalic acid linker)

	ΔE/kJ mol^{-1}		ΔH_{30}/kJ mol^{-1}	
	CO_2	CH_4	CO_2	CH_4
TA	−13.3	−11.0	−9.8	−5.9
NH_2–TA	−19.1	−12.4	−14.8	−7.2
MIL-47	−24.7	−13.2	—	—
NH_2-MIL-47	−25.6	−14.5	—	—

and the other linkers in the framework. For the periodic calculations the adsorption enthalpies have not been calculated in view of the difficulties encountered in the VASP calculations to obtain positive frequencies. To get an idea about the position of the CO_2 adsorbate in the periodic structure we refer to Fig. 11. Compared to the geometry obtained using the small cluster calculations CO_2 now takes a configuration in between the amino group of the one linker and the aromatic nucleus of another linker.

Summarizing, we have shown that the experimental adsorption enthalpies obtained from pulse chromatographic experiments (Table 2) follow the same trend as the corresponding adsorbate–linker interactions. Also within the framework, our geometrically similar adsorption spots show the same trend. We can thus conclude that the difference in the linker–adsorbate interaction is the main driving force between CO_2/CH_4 separation within MIL-47 and MIL-47-NH_2 rather than an interaction with the amino groups. On specific MOFs, presence of NH_2 indirectly enhances CO_2 adsorption. In particular, for NH_2-MIL-53(Al), the amino groups play a key role in framework flexibility, and lead to the closure of the NH_2-MIL-53(Al) pores, hereby enhancing CO_2 adsorption due to stronger aspecific interactions on the one hand and exclusion of CH_4 molecules on the other hand.[45] Since MIL-47 and NH_2-MIL-47 are rather rigid and non-flexible, presence of amino groups does not result in pore contraction, and accordingly not in an increased CO_2 affinity either.

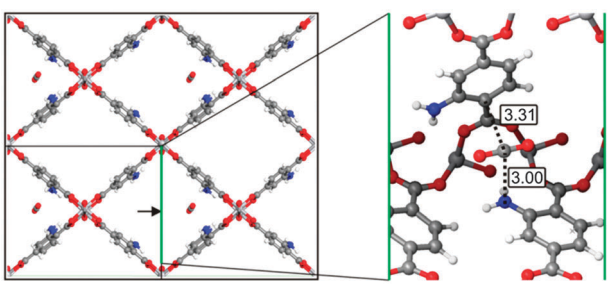

Fig. 11 Most stable adsorption position of CO_2 in the periodic structure of NH_2-MIL-47. Distances displayed in Ångström.

4. Conclusions

An amino functionalized V-MOF, with MIL-47 topology, has been successfully synthesized *via* both autoclave and microwave enhanced irradiation. The NH_2-MIL-47 shows a similar thermal stability in comparison to the parent MIL-47, decomposing in one step at 280 °C. An optimization of the exchange procedure in DMF was performed, resulting in a Langmuir surface area of approximately 672 m^2 g^{-1}. CO_2 and CH_4 adsorption measurements have shown that the presence of additional NH_2 groups does not have a beneficial effect on the adsorption properties, which was also confirmed by the theoretical modeling results. For the NH_2-MIL-47, both experiment and theory clearly show that the amination of the linker does not result in an increased adsorption capacity per mass of adsorbent, nor in an increased CH_4/CO_2 separation factor. The slight increase in adsorption enthalpy for the NH_2-MIL-47 does not compensate for the loss in pore volume compared to the parent MIL-47. In contrast to other MOFs, the NH_2-MIL-47 and the MIL-47 are not triggered into breathing behavior under the experimental conditions.

Acknowledgements

The authors acknowledge Dr. Els Bruneel for the XPS measurements and Danny Vandeput and Tom Planckaert for their aid in the N2-sorption, CHNS analysis and XRD measurements. Karen Leus is grateful to the Long Term Structural Methusalem Grant No. 01M00409 Funding by the Flemish Government. Furthermore, this research is co-funded by the Ghent University, GOA Grant No. 01G00710, BELSPO in the frame of IAP 6/27 and the European Research Council (FP7(2007-2013) ERC Grant No. 240483). Computational resources (Stevin Supercomputer Infrastructure) and services were provided by Ghent University. Joeri Denayer is grateful to the Hercules foundation for funding for medium-scale research infrastructure.

References

1 Y. H. Hu and L. Zhang, *Adv. Mater.*, 2010, **22**, E117–E130.
2 J. R. Li, Y. G. Ma, M. C. McCarthy, J. Sculley, J. M. Yu, H. K. Jeong, P. B. Balbuena and H. C. Zhou, *Coord. Chem. Rev.*, 2011, **255**, 1791–1823.
3 S. Q. Ma and H. C. Zhou, *Chem. Commun.*, 2010, **46**, 44–53.
4 L. J. Murray, M. Dinca and J. R. Long, *Chem. Soc. Rev.*, 2009, **38**, 1294–1314.
5 Z. Chang, D. S. Zhang, Q. Chen, R. F. Li, T. L. Hu and X. H. Bu, *Inorg. Chem.*, 2011, **50**, 7555–7562.
6 S. M. Xie, Z. J. Zhang, Z. Y. Wang and L. M. Yuan, *J. Am. Chem. Soc.*, 2011, **133**, 11892–11895.
7 Y. Ling, Z. X. Chen, H. Zheng, Y. M. Zhou, L. H. Weng and D. Y. Zhao, *Cryst. Growth Des.*, 2011, **11**, 2811–2816.

8 Y. G. Zhao, H. H. Wu, T. J. Emge, Q. H. Gong, N. Nijem, Y. J. Chabal, L. Z. Kong, D. C. Langreth, H. Liu, H. P. Zeng and J. Li, *Chem.–Eur. J.*, 2011, **17**, 5100–5108.
9 M. T. Luebbers, T. J. Wu, L. J. Shen and R. I. Masel, *Langmuir*, 2010, **26**, 11319–11329.
10 L. Alaerts, M. Maes, P. A. Jacobs, J. F. M. Denayer and D. E. De Vos, *Phys. Chem. Chem. Phys.*, 2008, **10**, 2979–2985.
11 L. Alaerts, C. E. A. Kirschhock, M. Maes, M. A. van der Veen, V. Finsy, A. Depla, J. A. Martens, G. V. Baron, P. A. Jacobs, J. E. M. Denayer and D. E. De Vos, *Angew. Chem., Int. Ed.*, 2007, **46**, 4293–4297.
12 X. L. Si, C. L. Jiao, F. Li, J. Zhang, S. Wang, S. Liu, Z. B. Li, L. X. Sun, F. Xu, Z. Gabelica and C. Schick, *Energy Environ. Sci.*, 2011, **4**, 4522–4527.
13 J. M. Simmons, H. Wu, W. Zhou and T. Yildirim, *Energy Environ. Sci.*, 2011, **4**, 2177–2185.
14 J. Sculley, D. Q. Yuan and H. C. Zhou, *Energy Environ. Sci.*, 2011, **4**, 2721–2735.
15 D. A. Yang, H. Y. Cho, J. Kim, S. T. Yang and W. S. Ahn, *Energy Environ. Sci.*, 2012, **5**, 6465–6473.
16 S. Choi, T. Watanabe, T. H. Bae, D. S. Sholl and C. W. Jones, *J. Phys. Chem. Lett.*, 2012, **3**, 1136–1141.
17 H. Liu, Y. G. Zhao, Z. J. Zhang, N. Nijem, Y. J. Chabal, H. P. Zeng and J. Li, *Adv. Funct. Mater.*, 2011, **21**, 4754–4762.
18 J. P. S. Mowat, S. R. Miler, J. M. Griffin, V. R. Seymour, S. E. Ashbrook, S. P. Thompson, D. Fairen-Jimenez, A. M. Banu, T. Duren and P. A. Wright, *Inorg. Chem.*, 2011, **50**, 10844–10858.
19 F. N. Shi, A. R. Silva and J. Rocha, *J. Solid State Chem.*, 2011, **184**, 2196–2203.
20 F. X. L. I. Xamena, A. Abad, A. Corma and H. Garcia, *J. Catal.*, 2007, **250**, 294–298.
21 J. Gascon, U. Aktay, M. D. Hernandez-Alonso, G. P. M. van Klink and F. Kapteijn, *J. Catal.*, 2009, **261**, 75–87.
22 J. Lee, O. K. Farha, J. Roberts, K. A. Scheidt, S. T. Nguyen and J. T. Hupp, *Chem. Soc. Rev.*, 2009, **38**, 1450–1459.
23 D. Y. Hong, Y. K. Hwang, C. Serre, G. Ferey and J. S. Chang, *Adv. Funct. Mater.*, 2009, **19**, 1537–1552.
24 K. Leus, I. Muylaert, M. Vandichel, G. B. Marin, M. Waroquier, V. Van Speybroeck and P. Van der Voort, *Chem. Commun.*, 2010, **46**, 5085–5087.
25 K. Leus, M. Vandichel, Y. Y. Liu, I. Muylaert, J. Musschoot, S. Pyl, H. Vrielinck, F. Callens, G. B. Marin, C. Detavernier, P. V. Wiper, Y. Z. Khimyak, M. Waroquier, V. Van Speybroeck and P. Van Der Voort, *J. Catal.*, 2012, **285**, 196–207.
26 Y. Y. Liu, K. Leus, M. Grzywa, D. Weinberger, K. Strubbe, H. Vrielinck, R. Van Deun, D. Volkmer, V. Van Speybroeck and P. Van der Voort, *Eur. J. Inorg. Chem.*, 2012, 2819–2827.
27 D. Farrusseng, S. Aguado and C. Pinel, *Angew. Chem., Int. Ed.*, 2009, **48**, 7502–7513.
28 M. D. Allendorf, C. A. Bauer, R. K. Bhakta and R. J. T. Houk, *Chem. Soc. Rev.*, 2009, **38**, 1330–1352.
29 S. Keskin and S. Kizilel, *Ind. Eng. Chem. Res.*, 2011, **50**, 1799–1812.
30 M. Eddaoudi, J. Kim, N. Rosi, D. Vodak, J. Wachter, M. O'Keeffe and O. M. Yaghi, *Science*, 2002, **295**, 469–472.
31 S. Biswas, T. Ahnfeldt and N. Stock, *Inorg. Chem.*, 2011, **50**, 9518–9526.
32 M. Kandiah, M. H. Nilsen, S. Usseglio, S. Jakobsen, U. Olsbye, M. Tilset, C. Larabi, E. A. Quadrelli, F. Bonino and K. P. Lillerud, *Chem. Mater.*, 2010, **22**, 6632–6640.
33 H. Y. Huang, R. T. Yang, D. Chinn and C. L. Munson, *Ind. Eng. Chem. Res.*, 2003, **42**, 2427–2433.
34 N. Hiyoshi, K. Yogo and T. Yashima, *Microporous Mesoporous Mater.*, 2005, **84**, 357–365.
35 Y. Belmabkhout, R. Serna-Guerrero and A. Sayari, *Ind. Eng. Chem. Res.*, 2010, **49**, 359–365.
36 C. Chen, W. J. Son, K. S. You, J. W. Ahn and W. S. Ahn, *Chem. Eng. J.*, 2010, **161**, 46–52.
37 V. Zelenak, M. Badanicova, D. Halamova, J. Cejka, A. Zukal, N. Murafa and G. Goerigk, *Chem. Eng. J.*, 2008, **144**, 336–342.
38 A. C. C. Chang, S. S. C. Chuang, M. Gray and Y. Soong, *Energy Fuel*, 2003, **17**, 468–473.
39 J. R. Karra and K. S. Walton, *J. Phys. Chem. C*, 2010, **114**, 15735–15740.
40 A. R. Millward and O. M. Yaghi, *J. Am. Chem. Soc.*, 2005, **127**, 17998–17999.
41 B. Arstad, H. Fjellvag, K. O. Kongshaug, O. Swang and R. Blom, *Adsorption*, 2008, **14**, 755–762.
42 P. Serra-Crespo, E. V. Ramos-Fernandez, J. Gascon and F. Kapteijn, *Chem. Mater.*, 2011, **23**, 2565–2572.
43 W. Morris, B. Leung, H. Furukawa, O. K. Yaghi, N. He, H. Hayashi, Y. Houndonougbo, M. Asta, B. B. Laird and O. M. Yaghi, *J. Am. Chem. Soc.*, 2010, **132**, 11006–11008.
44 S. Couck, J. F. M. Denayer, G. V. Baron, T. Remy, J. Gascon and F. Kapteijn, *J. Am. Chem. Soc.*, 2009, **131**, 6326–6327.
45 E. Stavitski, E. A. Pidko, S. Couck, T. Remy, E. J. M. Hensen, B. M. Weckhuysen, J. Denayer, J. Gascon and F. Kapteijn, *Langmuir*, 2011, **27**, 3970–3976.
46 S. Couck, E. Gobechiya, C. E. A. Kirschhock, P. Serra-Crespo, J. Juan-Alcaniz, A. M. Joaristi, E. Stavitski, J. Gascon, F. Kapteijn, G. V. Baron and J. F. M. Denayer, *ChemSusChem*, 2012, **5**, 740–750.
47 T. Lescouet, E. Kockrick, G. Bergeret, M. Pera-Titus and D. Farrusseng, *Dalton Trans.*, 2011, **40**, 11359–11361.
48 T. K. Trung, I. Deroche, A. Rivera, Q. Y. Yang, P. Yot, N. Ramsahye, S. D. Vinot, T. Devic, P. Horcajada, C. Serre, G. Maurin and P. Trens, *Microporous Mesoporous Mater.*, 2011, **140**, 114–119.
49 H. Leclerc, T. Devic, S. Devautour-Vinot, P. Bazin, N. Audebrand, G. Ferey, M. Daturi, A. Vimont and G. Clet, *J. Phys. Chem. C*, 2011, **115**, 19828–19840.
50 T. Devic, F. Salles, S. Bourrelly, B. Moulin, G. Maurin, P. Horcajada, C. Serre, A. Vimont, J. C. Lavalley, H. Leclerc, G. Clet, M. Daturi, P. L. Llewellyn, Y. Filinchuk and G. Ferey, *J. Mater. Chem.*, 2012, **22**, 10266–10273.
51 A. Phan, A. U. Czaja, F. Gandara, C. B. Knobler and O. M. Yaghi, *Inorg. Chem.*, 2011, **50**, 7388–7390.
52 N. A. Khan, J. W. Jun, J. H. Jeong and S. H. Jhung, *Chem. Commun.*, 2011, **47**, 1306–1308.
53 N. Rosenbach, A. Ghoufi, I. Deroche, P. L. Llewellyn, T. Devic, S. Bourrelly, C. Serre, G. Ferey and G. Maurin, *Phys. Chem. Chem. Phys.*, 2010, **12**, 6428–6437.
54 K. Barthelet, J. Marrot, D. Riou and G. Ferey, *Angew. Chem., Int. Ed.*, 2001, **41**, 281–284.
55 A. Malek and S. Farooq, *J. Chem. Eng. Data*, 1996, **41**, 25–32.
56 R. A. Ocakoglu, J. F. M. Denayer, G. B. Marin, J. A. Martens and G. V. Baron, *J. Phys. Chem. B*, 2003, **107**, 398–406.
57 M. J. Frisch, G. W. Trucks, H. B. Schlegel, G. E. Scuseria, M. A. Robb, J. R. Cheeseman, G. Scalmani, V. Barone, B. Mennucci, G. A. Petersson, H. Nakatsuji, M. Caricato, X. Li, H. P. Hratchian, A. F. Izmaylov, J. Bloino, G. Zheng, J. L. Sonnenberg, M. Hada, M. Ehara, K. Toyota, R. Fukuda, J. Hasegawa, M. Ishida, T. Nakajima, Y. Honda, O. Kitao, H. Nakai, T. Vreven, J. A. Montgomery, Jr., J. E. Peralta, F. Ogliaro, M. Bearpark, J. J. Heyd, E. Brothers, K. N. Kudin, V. N. Staroverov, R. Kobayashi, J. Normand, K. Raghavachari, A. Rendell, J. C. Burant, S. S. Iyengar, J. Tomasi, M. Cossi, N. Rega, N. J. Millam, M. Klene, J. E. Knox, J. B. Cross, V. Bakken, C. Adamo, J. Jaramillo, R. Gomperts, R. E. Stratmann, O. Yazyev, A. J. Austin, R. Cammi, C. Pomelli, J. W. Ochterski, R. L. Martin, K. Morokuma, V. G. Zakrzewski, G. A. Voth, P. Salvador, J. J. Dannenberg, S. Dapprich, A. D. Daniels, O. Farkas, J. B. Foresman, J. V. Ortiz, J. Cioslowski and D. J. Fox, *Gaussian 09, Revision A.02*, Gaussian, Inc., Wallingford CT, 2009.
58 Y. Zhao and D. G. Truhlar, *Theor. Chem. Acc.*, 2008, **120**, 215–241.
59 Y. Zhao and D. G. Truhlar, *Acc. Chem. Res.*, 2008, **41**, 157–167.
60 S. Grimme, *J. Comput. Chem.*, 2004, **25**, 1463–1473.
61 S. Grimme, J. Antony, S. Ehrlich and H. Krieg, *J. Chem. Phys.*, 2010, **132**, 15410.
62 A. Ghysels, T. Verstraelen, K. Hemelsoet, M. Waroquier and V. Van Speybroeck, *J. Chem. Inf. Model.*, 2010, **50**, 1736–1750.
63 G. Kresse and J. Hafner, *Phys. Rev. B: Condens. Matter Mater. Phys.*, 1994, **49**, 14251–14269.
64 G. Kresse and J. Hafner, *Phys. Rev. B: Condens. Matter Mater. Phys.*, 1993, **47**, 558–561.
65 G. Kresse and J. Furthmuller, *Phys. Rev. B: Condens. Matter Mater. Phys.*, 1996, **54**, 11169–11186.
66 G. Kresse and J. Furthmuller, *Comput. Mater. Sci.*, 1996, **6**, 15–50.

67 J. P. Perdew, K. Burke and M. Ernzerhof, *Phys. Rev. Lett.*, 1996, **77**, 3865–3868.
68 J. P. Perdew, K. Burke and M. Ernzerhof, *Phys. Rev. Lett.*, 1997, **78**, 1396.
69 T. Devic, P. Horcajada, C. Serre, F. Salles, G. Maurin, B. Moulin, D. Heurtaux, G. Clet, A. Vimont, J. M. Greneche, B. Le Ouay, F. Moreau, E. Magnier, Y. Filinchuk, J. Marrot, J. C. Lavalley, M. Daturi and G. Ferey, *J. Am. Chem. Soc.*, 2010, **132**, 1127–1136.
70 B. Jarrais, A. R. Silva and C. Freire, *Eur. J. Inorg. Chem.*, 2005, 4582–4589.
71 *Interpretation of Infrared Spectra, A Practical Approach*, J. Coates, 2000.
72 T. Loiseau, C. Serre, C. Huguenard, G. Fink, F. Taulelle, M. Henry, T. Bataille and G. Ferey, *Chem.–Eur. J.*, 2004, **10**, 1373–1382.
73 S. Bourrelly, P. L. Llewellyn, C. Serre, F. Millange, T. Loiseau and G. Ferey, *J. Am. Chem. Soc.*, 2005, **127**, 13519–13521.
74 J. F. M. Denayer and G. V. Baron, *Adsorption*, 2005, **11**, 85–90.
75 S. Couck, T. Remy, G. V. Baron, J. Gascon, F. Kapteijn and J. F. M. Denayer, *Phys. Chem. Chem. Phys.*, 2010, **12**, 9413–9418.
76 N. A. Ramsahye, G. Maurin, S. Bourrelly, P. L. Llewellyn, C. Serre, T. Loiseau, T. Devic and G. Ferey, *J. Phys. Chem. C*, 2008, **112**, 514–520.
77 N. A. Ramsahye, G. Maurin, S. Bourrelly, P. L. Llewellyn, T. Devic, C. Serre, T. Loiseau and G. Ferey, *Adsorption*, 2007, **13**, 461–467.
78 J. M. Castillo, T. J. H. Vlugt and S. Calero, *J. Phys. Chem. C*, 2009, **113**, 20869–20874.
79 L. Vanduyfhuys, T. Verstraelen, M. Vandichel, M. Waroquier and V. Van Speybroeck, *J. Chem. Theory Comput.*, 2012, **8**, 3217–3231.